A Vaccination and Isolation Strategy Based on an Adaptive Sliding Mode Control Design for the COVID-19 Virus (Omicron Variant) in Jakarta, Indonesia

Dewi Suhika[1,2,*], **Roberd Saragih**[1], **Dewi Handayani**[1], **Mochamad Apri**[1]

[1]Departement of Mathematics, Institut Teknologi Bandung, Bandung 40132, Indonesia
[2]Mathematics Study Program, Institut Teknologi Sumatera, Lampung 35365, Indonesia

[*]Email: 30120006@mahasiswa.itb.ac.id

Abstract

The Omicron variant, identified as B.1.1.529, has been recognized as a variant of concern (VOC) by the World Health Organization (WHO), necessitating continuous monitoring and a proactive response. This study develops a mathematical model to analyze the spread of COVID-19 mutations, considering a population that, despite vaccination, remains susceptible to infection. The model also accounts for key epidemiological factors, including the incubation period, quarantine measures, and various intervention strategies. This study focuses on the epidemiological conditions in Jakarta Province, where the highest number of Omicron cases in Indonesia has been recorded. Real-world epidemiological data related to Omicron in Jakarta were collected between February 6, 2022, and May 6, 2022. Model parameters were estimated using genetic algorithm optimization. A significant challenge in epidemic modeling is the uncertainty of parameters, which can substantially affect the effectiveness of control measures. To address this challenge, an adaptive sliding mode control approach is introduced, allowing dynamic adjustments to parameter variations without requiring precise parameter estimation. This approach maintains system stability by enforcing a predefined sliding surface, making it inherently robust against uncertainties. The main goal of this approach is to gradually minimize infections attributed to the initial COVID-19 strain and the Omicron variant, while simultaneously decreasing the count of susceptible individuals by ensuring the system follows a specified reference trajectory. Additionally, an adaptive mechanism is implemented to account for unknown variations in the system using the Lyapunov stability theorem. Numerical simulations illustrate that adaptive sliding mode control significantly improves epidemic management, reducing infections by 92.8% for the original strain and by 96.87% for the Omicron variant when compared to an uncontrolled scenario. Furthermore, the basic reproduction number (R_0) is lowered by 85.92%, confirming the efficiency of adaptive sliding mode control in mitigating the outbreak. Moreover, this study incorporates a cost-effectiveness analysis to assess the viability of various vaccination and isolation strategies. The findings contribute to epidemiological research by offering valuable insights for policymakers in designing effective and resilient intervention strategies for epidemic management.

Keywords: COVID-19, Omicron, control strategy, sliding mode control, adaptive
2020 MSC classification number: 93C10, 92D30, 93D20, 93C40

1. INTRODUCTION

Omicron (B.1.1.529) represents a newly emerged strain of the COVID-19 virus, characterized by its higher transmissibility and its impact on immune response acquired from previous infection or vaccination. Initially identified in South Africa on 24 November 2021 [1], the variant has since spread globally, including to Indonesia [2]. The world Organization (WHO) has labeled Omicron as a Variant of Concern (VOC), which refers to a strain of the coronavirus that may lead to increased transmission and mortality, and potentially influence vaccine efficacy. This categorization stemmed from the identification of numerous genetic alterations within the strain, several of which raised notable concerns. Preliminary analyses revealed that Omicron could pose a heightened likelihood of reinfection compared to prior VOCs, including Alpha (B.1.1.7), Beta (B.1351), Gamma (P.1), and Delta (B.1.617.2). Moreover, Omicron has demonstrated a rapid rate of spread [3]. Based

*Corresponding author
Received July 2^{nd}, 2024, Revised February 11^{th}, 2025, Accepted for publication March 19^{th}, 2025. e-ISSN: 2549-2896, DOI:10.5614/cbms.2025.8.1.2

on this, the Omicron variant is predicted to adversely impact the epidemiology of the virus. Although most countries have promoted vaccination, the epidemic has not been effectively reduced or controlled [4].

Mathematical models can be used as tools to study the dynamics of disease epidemics. Several studies related to the COVID-19 epidemic have been developed by researchers. In the initial stages of the COVID-19 pandemic, epidemiologists employed a range of mathematical models to gain insight into the virus's transmission patterns, the infection rate, and its consequences for populations. Khan et al. [5] established an SEIR framework to examine early cases in Wuhan, with a focus on interactions at seafood markets as the primary source of infection. They presented both a simple model and a fractional model, with numerical solutions providing insights for infection control. Li et al. [6] developed an SEIR model to assess Wuhan's handling of the COVID-19 outbreak and to investigate the effects of essential non-pharmaceutical interventions (NPIs) enforced throughout the outbreak. Along with the development of the vaccine, Liu et al. [7] developed an SEIR model by adding individual compartments to be vaccinated. In addition, an SEIR mathematical model focusing on the Omicron variant has been developed by [1]. The framework provides graphical results for models with susceptible parameters, underscoring that adherence to the World Health Organization's (WHO) guidance, including practices such as social distancing, mask-wearing, and hand hygiene can substantially reduce population infection rates.

Within the framework of mathematical modeling, determining parameter values is a critical factor requiring precise estimation for predictive accuracy. Genetic Algorithms, an innovative method, provide a solution enabling exploration of a broader parameter space through a population-based approach, utilizing genetic variation and processing techniques such as crossing over and mutation [8]. The advantage of genetic algorithms lies in their ability to operate independently of gradient evaluations of the objective function, in contrast to more conventional approaches [9]. Lambora et al. [8] recommend genetic algorithms as a preferred approach, particularly when dealing with problems featuring dual goals or constraints, as the algorithms have proven to be highly effective in extensive search spaces with numerous parameters. Yarsky [10] and Qiu et al. [11] discuss the application of genetic algorithms in identifying unknown parameters in the SEIR model and the impact on COVID-19 models. Therefore, in this study, we propose the implementation of a genetic algorithm to address challenges in estimating unknown parameters in the development of an SEIR model, thereby facilitating a deeper understanding of the Omicron variant's role in the spread of COVID-19 and formulating more effective control strategies.

Robust control strategies have become increasingly prominent in epidemic modeling because of their effectiveness in parameters and external disruptions [12]. Among these, sliding mode control is commonly applied to maintain system stability by guiding trajectories along a predefined surface, even in the presence of uncertain condition [13]. Several studies have demonstrated its effectiveness in epidemiological models. Jiao et al. [14] proposed a control strategy incorporating vaccination into a sliding mode control framework to regulate disease transmission within a generalized SEIR-type epidemic setting. Their results showed that this method effectively reduced infection rates by dynamically adjusting control inputs in response to changing epidemiological conditions. Similarly, Assegaf et al. [15] applied a sliding mode control strategy with adaptive features to mathematical model of cholera transmission. The method included dynamic adjustment of control gain in real time to effectively address parameter uncertainty. Another study by Santos et al. [16] highlighted the role of sliding mode control in managing quarantined populations, showing that it provides a robust framework for epidemic control under uncertain transmission dynamics. Furthermore, Ibeas et al. [17] proposed a robust vaccination controller for an SEIR model, demonstrating how modifications to traditional sliding mode control, such as improved control laws, can enhance robustness and reduce chattering effects. Their findings further support the viability of robust sliding mode-based control strategies in epidemic management.

Despite the advantages of sliding mode control, many existing implementations rely on fixed control gains, which limit adaptability in dynamic epidemic environments. Epidemic models inherently suffer from parameter uncertainty, arising from variations in disease transmission rates, intervention effectiveness, and population behavior. Control strategies that assume fixed parameters may require frequent re-calibration to remain effective, which can be impractical for real-time epidemic management. To address this challenge, this study introduces an adaptive sliding mode control approach that dynamically adjusts control parameters in real time, ensuring greater robustness in epidemic control.

The novelty of this study lies in integrating adaptive sliding mode control with epidemiological modeling to effectively manage parameter uncertainty while fulfilling specific control objectives. Sliding mode control

ensures global stability, while adaptive methods enable continuous monitoring and adaptation of system parameters over time. The combination of these two approaches enhances system performance and ensures robustness against uncertainties and disturbances. Unlike traditional sliding mode control methods with fixed parameters, adaptive sliding mode control dynamically adjusts the switching gain to compensate for unknown variations in transmission rates and intervention effectiveness. This method ensures that the epidemic system remains stable and follows a predefined reference trajectory, reducing infections without requiring precise parameter estimation.

In addition to the control design, this research evaluates both the epidemiological and economic impact of the proposed adaptive sliding mode control strategy. Specifically, the basic reproduction number (R_0) is compared before and after the implementation of control measures to assess the effectiveness of adaptive sliding mode control in limiting disease transmission. Furthermore, a cost-effectiveness analysis is conducted to determine the feasibility of different vaccination and isolation strategies. This analysis considers both the cost-effectiveness ratio (CER) and the incremental cost-effectiveness ratio (ICER) to evaluate the economic viability of interventions using adaptive sliding mode control in comparison to other strategies.

By incorporating epidemiological modeling, robust adaptive control strategies, and economic assessment, this study provides critical insights into the practical implementation of adaptive sliding mode control in epidemic management and public health decision-making. The results emphasize the importance of real-time gain adaptation in managing epidemic outbreaks, offering a flexible and resilient approach for policymakers and health authorities to design cost-effective and robust intervention strategies.

The organization of this study is presented as follows. Section 2 outlines a detailed explanation of the COVID-19 model used for the Omicron variant and describes the estimation process for several unknown parameters using epidemiological data from DKI Jakarta Province. Section 3 elaborates on how a sliding mode control approach is tailored adaptively to manage the dynamics of the Omicron variant. Section 4 provides the results and numerical simulations to evaluate the control strategy's performance. Finally, Section 5 summarizes the key findings and final insights from the study.

2. MATHEMATICAL MODELING

This part introduces the construction of mathematical framework to simulate the spread of the Omicron variant within vaccinated populations. Several model parameters are determined through genetic algorithm optimization based on real-world data. Estimating these parameters is essential for gaining insights into the spread and behavior of this variant, as well as for designing effective intervention strategies.

2.1. Mathematical model of the original virus and Omicron variant

This section by outlining several key assumptions, followed by the formulation of a new mathematical model that captures the transmission behavior of the Omicron variant of COVID-19. The development of this model is inspired by the structure in [1] and is further extended by introducing additional compartments, including vaccinated individuals, quarantine units, individuals infected with the original strain, those infected with the Omicron variant, as well as vaccine efficacy and disease management strategies. The total population is segmented into eight categories, as illustrated in Figure 1: susceptible individuals (S), individuals in contact with the original virus (E), those who have encountered the Omicron variant (E_m), vaccinated individuals (V), those infected with the original virus (I), infected with Omicron (I_m), quarantined individuals (Q), and recovered individuals (R). A detailed explanation of each parameter is provided in Table 1.

In the model, assumptions are incorporated as constraints to aid in structuring the model. The assumptions are as follows:

(i) It is assumed that the number of births matches the natural mortality rate, leading to a stable total population size. This assumption is commonly used in epidemic modeling to preserve analytical tractability while minimizing the influence of demographic variations on disease transmission patterns [18]. Over short periods, assuming a constant population does not significantly impact epidemiological outcomes, as birth and death rates tend to balance each other.

(ii) The population is assumed to be a closed system, meaning that no individuals enter or leave the observed area [20].
(iii) All newborns are classified as susceptible upon birth. Unless they receive protection from maternal antibodies, they are generally at risk of contracting infections as passive immunity gradually decreases over time [19].
(iv) Individuals who have been vaccinated but have not yet achieved full immunity may remain susceptible to infection. If the vaccine does not provide complete protection, there is still a possibility that vaccinated individuals could contract the disease [21].
(v) Transmission of the Omicron variant occurs primarily via close contact with persons already infected by strain. In contrast, the original strain tends to spread when uninfected individuals are exposed to carriers of the initial virus. Importantly, encountering someone infected with the original strain could result in transmission; however, this does not automatically imply contraction of the Omicron. [22].
(vi) The spread of the virus occurs due to interactions between individuals who are susceptible and those who have already been infected [23].
(vii) Individuals who were previously diagnosed as COVID-19 positive and have subsequently recovered are assumed to have developed immunity against reinfection [24].

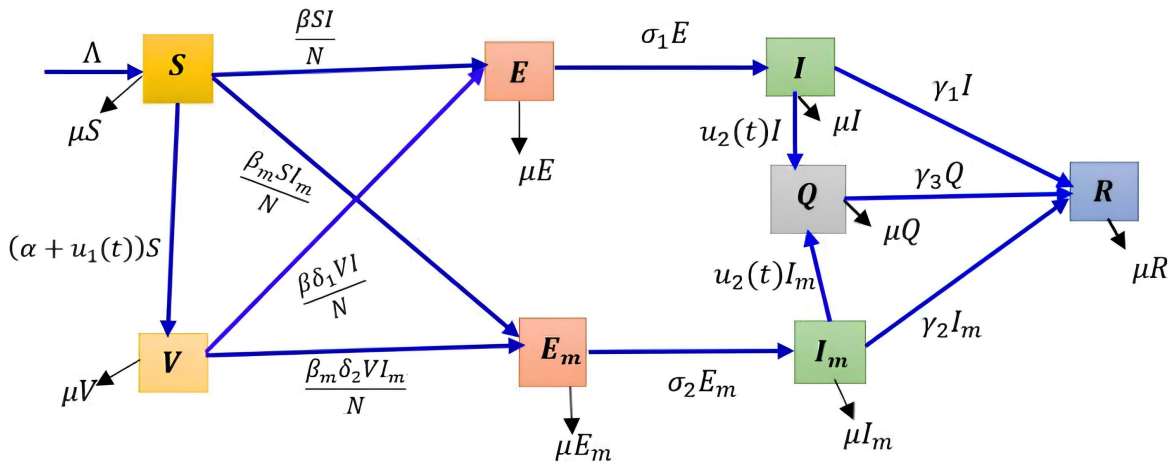

Figure 1: Schematic representation of COVID-19 transmission pathways.

Susceptible Compartment, S: The growth of the susceptible compartment is modeled under the assumption that the total population remains constant, with a birth rate of Λ individuals per day. The Susceptible sub population decreases due to moving to E and E_m compartments as a result of interacting with infected individuals I and I_m with infection rates β and β_m, respectively, so that the transmission rates are $\frac{\beta SI}{N}$ and $\frac{\beta_m I_m}{N}$. The death rate μ of susceptible individuals S per day is denoted as μS per day. The movement of individuals from compartment S to V is due to the increased rate of vaccinated individuals and is given by $\alpha\ S$. Thus, the change in the population in the S compartment with respect to time is:

$$\frac{dS(t)}{dt} = \Lambda - \frac{\beta S(t)I(t)}{N} - \frac{\beta_m I_m(t)S(t)}{N} - \alpha S(t) - \mu S(t).$$

Compartment containing individuals in contact with the original virus, E: The addition to compartment E is caused by the movement of individuals from compartment S to E as a result of interacting with infected individuals I with an infection rate β. Thus, the transmission rate is $\frac{\beta SI}{N}$ per day. The movement of individuals

from compartment V to E results from interacting with infected individuals I with an infection rate of β; the transmission rate is $\frac{\beta SI}{N}$ per day. The parameter δ_1 indicates the likelihood that vaccinated individuals fail to produce antibodies against the initial strain after 28 days. The population in compartment E declines due to two factors: transition to compartment I, represented by the rate $\delta_1 E$, and natural mortality in E, quantified as μE per day. Thus,

$$\frac{dE(t)}{dt} = \frac{\beta S(t)I(t)}{N} + \frac{\beta\delta_1 V(t)I(t)}{N} - \delta_1 E(t) - \mu E(t).$$

Compartment of individuals who have been exposed to the Omicron variant, E_m: The number of individuals in the E_m compartment rises as susceptible individuals S interact with infected individuals I_m. The corresponding transmission is quantified by the rate $\beta_m S I_m N$ per day. Additionally, vaccinated individuals in V can transition to E_m when exposed to I_m, with a transmission rate of $\beta_m \delta_2 V I_m N$, where δ_2 represents the probability that vaccine does not confer immunity against the original strain within a 28-days period. The E_m compartment decreases at a transition rate of $\delta_2 E_m$, the population movement from compartment E_m to I_m, and the death rate in the E_m compartment per day denoted μ is μE_m per day. Thus, we have

$$\frac{dE_m(t)}{dt} = \frac{\beta_m S(t)I_m(t)}{N} + \frac{\beta_m\delta_2 V(t)I_m(t)}{N} - \delta_2 E_m(t) - \mu E_m(t).$$

Compartment of vaccinated individuals, V: The V compartment increases due to an increase in the vaccination rate α S. Meanwhile, individuals from the susceptible compartment S may move into this class. However, several mechanisms contribute to the reduction of individuals in V:

(a) Individuals may shift from the vaccinated compartment V to the exposed class E upon interacting with infected persons in class I, where the transmission rate is β. Hence, the corresponding transmission rate become $\frac{\beta\delta_1 VI}{N}$ per day, where δ_1 denotes the likelihood that vaccinated individuals fail to develop immunity against the original strain within 28 days.

(b) Similarly, exposure to infected individuals carrying the Omicron variant (I_m) can cause a transition from V to E_m, with an infection rate of β_m. The resulting rate is $\frac{\beta_m\delta_2 V I_m}{N}$ per day, where δ_2 reflects the chance that vaccine-induced immunity does not protect against the original virus after 28 days.

(c) The daily mortality within the vaccinated compartment V is modeled as μV, where μ is the death rate.

Accordingly, the dynamic behavior of the vaccinated compartment V over time can be modeled by the following expression:

$$\frac{dV(t)}{dt} = \alpha S(t) - \frac{\beta\delta_1 V(t)I(t)}{N} + \frac{\beta_m\delta_2 V(t)I_m(t)}{N} - \mu V(t).$$

Compartments of individuals who have contacted the original virus, I: Infected individuals due to the original virus, represented by compartment I, experience an increase in population as individuals transition from the exposed class E to I, at rate governed by σ_1 E. The number in compartment I declines through tree main mechanisms: natural mortality, occurring at a rate of μI per day, recovery of individuals from I to R, represented by the term γ_1 I, and movement into quarantine Q through isolation strategies, occurring at the rate u_2 I. Accordingly, the variation in the number of individuals in compartment I over time can be expressed as:

$$\frac{dI(t)}{dt} = \sigma_1 E(t) - u_2 I(t) - \gamma_1 I(t) - \mu I(t).$$

Compartment I_m**, representing individuals infected by the Omicron variant**: The I_m compartment increases due to the transition with the rate $\sigma_2 E_m$, the individual displacement from compartment E_m to I_m. Compartment I_m is reduced due to death at the rate I_m per day and is thus denoted μ of μI_m per day, transfer to the isolation compartment Q at a rate $u_2 I_m$, and recovery into the recovered class R governed by $\gamma_2 I_m$. Accordingly, the dynamic change of I_m over time can be expressed as follows:

$$\frac{dI_m(t)}{dt} = \sigma_2 E_m(t) - u_2 I_m(t) - \gamma_2 I_m(t) - \mu I_m(t).$$

Compartment of quarantined individuals, Q: The Q compartment increases due to isolation at the rates $u_2 I$ and $u_2 I_m$. The Q compartment is reduced by deaths in compartment I and is denoted μ by μI per day, and the recovery rate is γ_3 Q. Thus, the change in compartment Q over time is:

$$\frac{dQ(t)}{dt} = u_2 I(t) + u_2 I_m(t) - \gamma_3 Q(t) - \mu Q(t).$$

Compartment of recovered individuals, R: The number of individuals in compartment R increases as people transition from the infected compartments to the recovered state. Specifically, individuals move from compartment I to R at the recovery rate of $\gamma_1 I$, from I_m to R at γ_2 I_m, and from Q to R at a recovery rate of $\gamma_3 Q$. Additionally, the R compartment decreases due to natural mortality, represented by μR per day. Consequently, the rate of change in the recovered compartment over time is given by:

$$\frac{dR(t)}{dt} = \gamma_1 I(t) + \gamma_2 I_m(t) + \gamma_3 Q(t) - \mu R(t).$$

There are two control functions incorporated in this model. The first, $u_1(t)$, represents vaccination efforts aimed at curbing the spread of COVID-19 by increasing the proportion of immunized individuals. The second control function, $u_2(t)$, represents isolation measures applied to I and I_m to limit the spread of infection within the population.

Building upon these definitions, a transmission diagram illustrating the mathematical model for COVID-19 dynamics is provided in Figure 1. The subsequent section presents the complete mathematical model incorporating control measures.

$$\begin{aligned}
\tfrac{\mathrm{d}S(t)}{\mathrm{d}t} &= \Lambda - \tfrac{\beta I(t) S(t)}{N} - \tfrac{\beta_m I_m(t) S(t)}{N} - (\alpha + u_1(t))\, S(t) - \mu S(t), \\
\tfrac{\mathrm{d}E(t)}{\mathrm{d}t} &= \tfrac{\beta S(t) I(t)}{N} + \tfrac{\beta \delta_1 V(t) I(t)}{N} - \sigma_1 E(t) - \mu E(t), \\
\tfrac{\mathrm{d}E_m(t)}{\mathrm{d}t} &= \tfrac{\beta_m S(t) I_m(t)}{N} + \tfrac{\beta_m \delta_2 V(t) I_m(t)}{N} - \sigma_2 E_m(t) - \mu E_m(t), \\
\tfrac{\mathrm{d}V(t)}{\mathrm{d}t} &= (\alpha + u_1(t))\, S(t) - \tfrac{\beta \delta_1 V(t) I(t)}{N} - \tfrac{\beta \delta_2 V(t) I_m(t)}{N} - \mu V(t), \\
\tfrac{\mathrm{d}I(t)}{\mathrm{d}t} &= \sigma_1 E(t) - u_2(t) I(t) - \gamma_1 I(t) - \mu I(t), \\
\tfrac{\mathrm{d}I_m(t)}{\mathrm{d}t} &= \sigma_2 E_m(t) - u_2(t) I_m(t) - \gamma_2 I_m(t) - \mu I_m(t), \\
\tfrac{\mathrm{d}Q(t)}{\mathrm{d}t} &= u_2(t) I(t) + u_2(t) I_m(t) - \gamma_3 Q(t) - \mu Q(t), \\
\tfrac{\mathrm{d}R(t)}{\mathrm{d}t} &= \gamma_1 I(t) + \gamma_2 I_m(t) + \gamma_3 Q(t) - \mu R(t).
\end{aligned} \tag{1}$$

The total population at any time $N(t)$ is determined as the sum of all compartments, $N(t) = S(t) + E(t) + E_m(t) + V(t) + I(t) + I_m(t) + Q(t) + R(t)$. By summing the differential equations governing the model, the total population follows the equation

$$\frac{dN}{dt} = \Lambda - \mu N.$$

where $\Lambda = bN$. Solving this differential equation, we obtain

$$N(t) = N_0 e^{(b-\mu)t}.$$

Given the assumption that the rate of birth b matches the natural mortality rate μ, we obtain

$$N(t) = N_0 e^{(0)t} = N_0.$$

This confirms that the total population remains unchanged over time when the birth and death rates are balanced.

Control function $u_1(t)$ and $u_2(t)$ represents vaccination and isolation. The set of allowable control functions is as follows

$$\varpi = \{(u_1(t), u_2(t) \mid 0 \leq u_1(t) \leq 1, 0 \leq u_2(t) \leq 1)\}.$$

The control input $u_1(t)$ is designed to reduce the susceptible population to COVID-19 by promoting a higher vaccination coverage. This approach helps curb disease transmission and enhances overall population immunity. The value of this control variable can range from 0 to 1, with 0 representing no vaccinations performed and 1 representing full vaccination or 100% of the population being vaccinated.

The isolation control $u_2(t)$ represents virus isolation measures applied to infected individuals, thereby curbing the transmission of both the original strain and the Omicron variant. The value of this control variable also ranges from 0 to 1, with 0 indicating no isolation measures and 1 indicating total isolation or strict social distancing. Increased isolation intensity help minimize interpersonal contact, thus mitigating disease spread though reduced social interactions. It is important to pay attention to the limits of control variable values (from 0 to 1) to maintain consistency and accurate interpretation in managing disease transmission.

2.2. Positivity and boundedness of solutions

Ensuring the system's validity from both mathematical and biological perspectives requires confirming that its solutions stay non-negative and within bounds. This part illustrates that every solution of system (1) retains non-negative throughout the time domain $t \geq 0$. The system can be generally expressed as follows:

$$\frac{dX}{dt} = G(X),$$

in which $X = (S, E, E_m, V, I, I_m, Q, R)$ defines the state variables, and $G(X)$ represents the vector-valued function that determines the right-hand side of the differential system given in Equation (1). For any compartment X_i let $\phi_i(X)$ represent the net flux of individuals entering or leaving that compartment. Given an initial condition $X_i(0) \geq 0$, its time evolution satisfies

$$X_i(t) = X_i(0) \exp\left(-\int_0^t \phi_i(u)du\right) + \int_0^t F_i(u) \exp\left(-\int_u^t \phi_i(z)dz\right) du,$$

Here $F_i(u)$ represents the inflow into the compartment. Since all transition rates in the model are assumed to be non-negative, it follows that $X_i(t) \geq 0$ for all $t \geq 0$, ensuring the positivity of the solutions.

To establish the boundedness of the solutions, consider the total population $N(t)$, which evolves according to

$$\frac{dN}{dt} = \Lambda - \mu N - dI_m.$$

Under the assumption that the disease-induced death rate d is small, an upper bound can be derived

$$\limsup_{t\to\infty} N(t) \leq \frac{\Lambda}{\mu},$$

As a results, the overall population size stays within a limited range for every $t \geq 0$. Therefore, every possible trajectory of the system lies within the biologically meaningful set of values.

$$\Omega = \left\{(S, E, E_m, V, I, I_m, Q, R) \in \mathbb{R}_+^8 \mid N \leq \frac{\Lambda}{\mu}\right\}.$$

Consequently, the model remains mathematically well-defined in a biological context, confirming that the solutions uphold both positivity and boundedness over time.

2.3. Reproduction number of the mathematical model

In the absence of infections within system (1), where $E(t) = E_m(t) = I(t) = I_m(t) = Q(t) = 0$, the equilibrium condition aligns with the Disease-Free Equilibrium (DFE), represented as

$$E_0 = \left(\frac{\Lambda}{\alpha + \mu}, 0, 0, \frac{\alpha\Lambda}{\mu(\alpha + \mu)}, 0, 0, 0, 0 \right).$$

This equilibrium signifies the steady-state scenario where the disease does not spread within the population. To determine the basic reproduction number R_0, the next-generation matrix approach is utilized. The infection dynamics of the model can be formulated using matrices F and $\mathcal{V}$, where F represents the new infections, and $\mathcal{V}$ represents transitions out of the infected compartments. The expression for the matrix F is formulated as follows

$$F = \begin{bmatrix} \frac{\beta SI}{N} + \frac{\beta\delta_1 VI}{N} \\ \frac{\beta_m SI_m}{N} + \frac{\beta_m\delta_2 VI_m}{N} \\ 0 \\ 0 \end{bmatrix}.$$

The matrix $\mathcal{V}$ is represented as

$$\mathcal{V} = \begin{bmatrix} \sigma_1 E + \mu E \\ \sigma_2 E_m + \mu E_m \\ -\sigma_1 E + u_2 I + \gamma_1 I + \mu I \\ -\sigma_2 E_m + u_2 I_m + \gamma_2 I_m + \mu I_m \end{bmatrix}.$$

The Jacobian matrices J_F and $J_{\mathcal{V}}$ evaluated at the DFE, E_0 are

$$J_F(E_0) = \begin{bmatrix} 0 & 0 & \frac{\Lambda\beta}{(\Lambda/(\alpha+\mu)+(\Lambda\alpha)/(\mu(\alpha+\mu)))(\alpha+\mu)} & 0 \\ 0 & 0 & 0 & \frac{\Lambda\beta_m}{(\Lambda/(\alpha+\mu)+(\Lambda\alpha)/(\mu(\alpha+\mu)))(\alpha+\mu)} \\ 0 & 0 & 0 & 0 \\ 0 & 0 & 0 & 0 \end{bmatrix},$$

$$J_{\mathcal{V}}(E_0) = \begin{bmatrix} \mu + \sigma_1 & 0 & 0 & 0 \\ 0 & \mu + \sigma_2 & 0 & 0 \\ -\sigma_1 & 0 & \gamma_1 + \mu + u_2 & 0 \\ 0 & -\sigma_2 & 0 & \gamma_2 + \mu + u_2 \end{bmatrix}.$$

The Next-Generation Matrix (G) is determined by the relationship:

$$G = J_F(E_0) \cdot J_{\mathcal{V}}^{-1}(E_0).$$

Substituting the values, we obtain

$$G = \begin{bmatrix} \frac{\beta\sigma_1}{(\mu+\sigma_1)(\gamma_1+\mu+u_2)} & 0 & \frac{\beta}{\gamma_1+\mu+u_2} & 0 \\ 0 & \frac{\beta_m\sigma_2}{(\mu+\sigma_2)(\gamma_2+\mu+u_2)} & 0 & \frac{\beta_m\delta_2}{\gamma_2+\mu+u_2} \\ 0 & 0 & 0 & 0 \\ 0 & 0 & 0 & 0 \end{bmatrix}.$$

The fundamental reproduction number, denoted as R_0, is mathematically expressed as

$$R_0 = \rho(G) = \max\left(R_{01}, R_{02}\right),$$

where $R_{01} = \frac{\beta\sigma_1}{(\mu+\sigma_1)(\gamma_1+\mu+u_2)}$ and $R_{02} = \frac{\beta_m\sigma_2}{(\mu+\sigma_2)(\gamma_2+\mu+u_2)}$. When $R_0 > 1$, the disease tends to fade out over time. On the other hand, If $R_0 < 1$, suggests that the disease will persist and spread further throughout the population.

2.4. Parameter estimation

Following the approach in [25], the genetic algorithm (GA) method is applied in multiple stages, including generating an initial population, evaluating fitness, selecting individuals, performing crossover, and introducing mutation. The next subsection presents the results of estimating unknown parameters in the COVID-19 model using GA. For the purpose of this estimation, data were gathered from the official website [26] within the time-frame of February 06, 2022, to May 06, 2022. This time-frame was chosen due to the significant rise in Omicron cases during that period.

To determine the natural death rate parameter, the reciprocal of the 2020 life expectancy, which is 70.69 years, is utilized. Based on this, the natural mortality rate is derived as $\mu = \frac{1}{70.69\times 365}$ [27]. For this study, the genetic algorithm was run for 40 iterations, using a population size of 100 and a selection rate of 0.5, and a mutation rate of 0.2. These configurations were set to enhance the accuracy of the parameter estimation process. To estimate these parameters, the fitness value (objective function) is evaluated through the Mean Absolute Percentage Error (MAPE), as described in the equation below.

$$\text{error} = \frac{1}{n_{\text{data}}} \sum_{i=1}^{n_{\text{data}}} \frac{x_i - x_i^*}{x_i},$$

where x_i represents the actual cumulative positive case data on day i, and x_i^* represents the estimated cumulative case data from ode45 on day i. In this study, the data used are cumulative positive COVID-19 case data from February 6, 2022, to May 06, 2022, resulting in a total of 91 data points, or $n_{\text{data}} = 91$. Table 1 presents the estimated parameter values obtained through the use of the genetic algorithm.

Table 1: The description of variable and parameter.

Notations	Description	Value	References
β	Rate at which the original virus is transmitted between individuals	0.10489	estimated
β_m	Rate characterizing Omicron transmission among individuals	0.17881	estimated
α	Vaccination rates	0.19566	estimated
δ_1	The probability that the recipient of the vaccine injection has not developed antibodies against the original virus after 28 days	0.05	[29]
δ_2	The probability that the recipient of the vaccine injection has not developed antibodies against the original virus after 28 days	0.33	[30]
σ_1	Rate at which an exposed person transitions from E to I	0.068593	estimated
σ_2	Transition rate of individuals from Omicron exposed state E_m to I_m	0.40599	estimated
γ_1	Rate of recovery for those in the infected compartment I	0.088527	estimated
γ_2	Rate of recovery for individuals infected with the Omicron variant I_m	0.081869	estimated
γ_3	Recovery rate for individuals in Q	0.071954	estimated
Λ	Recruitment rate	$N \times b$	[27]
b	Birth rate	$\frac{1}{70.36\times 365}$	[27]
μ	Natural death rate	$\frac{1}{70.36\times 365}$	[27]

In order to assess the model's precision, a validation process was performed by analyzing numerical simulation results against real recorded data. The following comparison demonstrates the extent to which the predicted infected population from simulations corresponds to the observed data, as shown in Figure 2.

The genetic algorithm produced a fairly good estimated value with a relatively small numerical error of 0.003354, and thus it can be concluded that the COVID-19 distribution model is suitable for describing conditions in the field with the given parameter values. The results of this parameter estimation will then be used in the next stage, namely the completion of the sliding mode control and numerical simulation of the application of the control.

3. Implementation of adaptive sliding mode strategy in a COVID-19 transmission model

This section considers the COVID-19 model presented in Equation (1), incorporating parameter uncertainties in β, β_m, σ_1, and γ_1. The adaptive sliding mode control strategy works by guiding the system toward

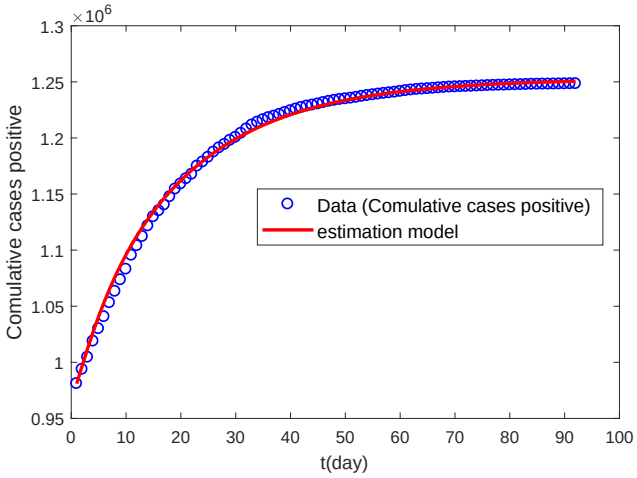

Figure 2: Graph of comparison of estimation results with real data.

a reference function, leading to a reduction in the infected populations $I(t)$ and $S(t)$. The stability of the proposed control method is ensured through the Lyapunov stability theorem.

3.1. Design of the sliding mode control

The development of the sliding mode control follows these steps.

Step 1. Establish the tracking errors $e_1(t)$ and $e_2(t)$, which represent deviations in the susceptible and infected compartments.

$$\begin{aligned} e_1(t) &= S(t) - S_d(t), \\ e_2(t) &= I(t) - I_d(t). \end{aligned}$$

where $S_d(t)$ and $I_d(t)$ serve as the reference functions for $S(t)$ and $I(t)$, respectively, ensuring compliance with the subsequent equation.

$$S_d(0) = S(0), S_d(t) \to 0, \tag{2}$$
$$I_d(0) = I(0), I_d(t) \to 0. \tag{3}$$

In Equation (2), the initial tracking error is considered to be zero, with $e_1(0) = 0$ and $e_2(0) = 0$. Meanwhile, Equation (3) indicates that the reference function gradually decreases toward zero as time progresses. The goal of the simulation is determined by the reference function given below.

$$S_d(t) = (S(0) - S(t_f)) \exp(-\varepsilon t) + S(t_f), \tag{4}$$
$$I_d(t) = (I(0) - I(t_f)) \exp(-\varepsilon t) + I(t_f) \ . \tag{5}$$

In this context, $S(t_f)$ and $I(t_f)$ represent the accumulated values of individuals who remain susceptible and those who are infected at the conclusion of the simulation period, considering the parameter $\varepsilon > 0$. The reference function related to COVID-19 transmission follows a mathematical model, which characterizes the optimal disease spread scenario or the intended objective for minimizing infection cases.

Step 2. Define the sliding variables $\phi_1(t)$ and $\phi_2(t)$ that fulfill the following control objectives:

$$\begin{aligned} \phi_1(t) &= e_1(t), \\ \phi_2(t) &= e_2(t). \end{aligned}$$

In this paper, we used a sliding surface with the equations

$$\begin{aligned}\phi_1(t) &= e_1(t) = 0,\\ \phi_2(t) &= e_2(t) = 0,\end{aligned}$$

to ensure the achievement of control objectives. To maintain the state in sliding mode, we ensure that $\phi_1(t) = \dot{\phi_1}(t) = 0$ and $\phi_2(t) = \dot{\phi_2}(t) = 0$ are applied. Proper sliding surfaces are designed to ensure that the system remains within the desired operational area and follows the desired control response.

Step 3. Define equivalent controls. Substituting $\phi_1(t) = 0$ and $\phi_2(t) = 0$ into Equation (4) and (5), we obtain the control values $u_1(t)$ and $u_2(t)$ that are then referred to as equivalent controls.

$$u_{1_{eq}} = \frac{1}{S(t)}\left(\Lambda - \left(\frac{\beta I(t)}{N} + \frac{\beta_m I_m(t)}{N} + \alpha + \mu\right) S(t)\right) + \frac{1}{S(t)}\left(\varepsilon\left(S(0) - S(t_f)\right)\exp\left(-\varepsilon t\right)\right), \tag{6}$$

$$u_{2_{eq}} = \frac{1}{I(t)}\left(\sigma_1 E(t) - \left(\gamma_1 + \mu\right) I(t)\right) + \frac{1}{I(t)}\left(\varepsilon\left(I(0) - I(t_f)\right)\exp\left(-\varepsilon t\right)\right). \tag{7}$$

The presence of uncertainty leads to the utilization of nominal and predefined parameters, since the exact system parameters are not known; therefore, we define

$$\begin{aligned} q &= \frac{\beta I(t)}{N} + \frac{\beta_m I_m(t)}{N} + \alpha + \mu, \qquad \hat{q} = \frac{\hat{\beta} I(t)}{N} + \frac{\hat{\beta_m} I_m(t)}{N} + \alpha + \mu,\\ s &= \gamma_1 + \mu, \qquad \hat{s} = \hat{\gamma_1} + \mu,\\ r &= \sigma_1 E(t), \qquad \hat{r} = \hat{\sigma_1} E(t),\end{aligned}$$

with $\hat{\beta}$, $\hat{\beta}$, $\hat{\gamma_1}$ and $\hat{\sigma_1}$ are nominal parameters of β, β_m, γ_1, and σ_1, so that the equivalent control in Equations (6) and (7) becomes

$$\hat{u}_{1_{eq}} = \frac{1}{S(t)}\left(\Lambda - \left(\hat{q} S(t) + \varepsilon\left(S(0) - S(t_f)\right)\exp\left(-\varepsilon t\right)\right)\right), \tag{8}$$

$$\hat{u}_{2_{eq}} = \frac{1}{I(t)}\left(\hat{r} - \left(\hat{s} I(t) + \varepsilon\left(I(0) - I(t_f)\right)\exp\left(-\varepsilon t\right)\right)\right). \tag{9}$$

Step 4. Define switching controls. Equivalent controls (8) and (9) are expanded nonlinearly to satisfy robust behavior with the selection of switching controls as follows

$$u_{1_{d(t)}} = \frac{1}{S(t)} g_1(x,t) sgn\left(\phi_1(t)\right), \tag{10}$$

$$u_{2_{d(t)}} = \frac{1}{S(t)} g_2(x,t) sgn\left(\phi_2(t)\right), \tag{11}$$

so the controller becomes

$$u_1(t) = \frac{1}{S(t)}\left(\Lambda - \left(\hat{q} S(t) + \varepsilon\left(S(0) - S(t_f)\right)\exp\left(-\varepsilon t\right)\right)\right) + \frac{1}{S(t)} g_1(x,t) sgn\left(\phi_1(t)\right), \tag{12}$$

$$u_2(t) = \frac{1}{I(t)}\left(\hat{r} - \left(\hat{s} I(t) + \varepsilon\left(I(0) - I(t_f)\right)\exp\left(-\varepsilon t\right)\right)\right) + \frac{1}{S(t)} g_2(x,t) sgn\left(\phi_2(t)\right). \tag{13}$$

The switching gain is established to address parameter uncertainty, ensuring that the control rules described in Equations (12) and (13) can produce the convergence of each tracking error. The definition of the switching gain is grounded in the following assumptions [28].

(i) There are state dependent functions $k(x,t)$ and $l(x,t)$ so that the following upper bounds are satisfied,

$$\mid (q - \hat{q}) S(t) \mid \leq k(x,t), \text{ and} \tag{14}$$

$$\mid r - \hat{r} + (s - \hat{s}) I(t) \mid \leq l(x,t). \tag{15}$$

(ii) The upper bound functions $k(x,t)$ and $l(x,t)$ are known.

(iii) Switching gains $g_1(x,t)$ and $g_2(x,t)$ are selected as

$$\begin{aligned} g_1(x,t) &= k(x,t) + c_1,\\ g_2(x,t) &= l(x,t) + c_2,\end{aligned}$$

where $c_1 > 0$ and $c_2 > 0$.

(iv) There exists finite, possibly unknown, positive constants $\bar{k}$ and $\bar{l}$ such that

$$\bar{k} \geq k(x,t), \tag{16}$$

$$\bar{l} \geq l(x,t). \tag{17}$$

Assumption (ii) implies that the upper bounds $k(x,t)$ and $l(x,t)$ are well-defined, following the typical convention in a sliding mode control system. Assumption (iii) guides the selection of the switching gains $g_1(x,t)$ and $g_2(x,t)$. Assumption (i) asserts that the upper bounds are dependent on the state function, while assumption (iv) specifies that $k(x,t)$ and $l(x,t)$ remain bounded by a constant.

Assumption (i) deals with the upper bounds of parameter uncertainty. The inclusion of $k(x,t)$ and $l(x,t)$ can be explained through how the model is structured using a particular parameter, even if its precise value is uncertain. The inequality (15) can be rewritten as

$$|(r-\hat{r})+(s-\hat{s})I(t)| \quad = \quad I(t)\left|u_{2actual}(t)-u_{2eq}(t)\right| \leq l(x,t). \tag{18}$$

Based on assumption (i), equation (18) shows that the application of the fluctuation isolation control considers the actual and nominal parameters limited by a certain upper bound function, thereby effectively handling errors arising from parameter uncertainties during the vaccination and isolation processes.

Proposition 3.1. *Given the system model in Equation (1) and applying the control laws in (12) and (13). If assumptions (i)-(iii) are met, then the tracking error will be asymptotically zero.*

Proof. Considering a candidate Lyapunov function based on the Lyapunov stability theorem

$$V(t) \quad = \quad \tfrac{1}{2}\left(\phi_1^2(t)+\phi_2^2(t)\right). \tag{19}$$

Taking the time derivative of Equation (19) and incorporating assumptions 1, 2, and 3, the following expression is derived:

$$\begin{aligned}
\dot{V}(t) &= \phi_1(t)\dot{\phi}_1(t)+\phi_2(t)\dot{\phi}_2(t) \\
&= \phi_1(t)\left(\Lambda-\frac{\beta S(t)I(t)}{N}-\beta_m S(t)I_m(t)N-(\alpha+u_1)\,S(t)-\mu S(t)+\varepsilon\,(S(0)-S(t_f))\,exp(-\varepsilon t)\right) \\
&\quad +\phi_2(t)\,(\sigma_1 E-u_2 I-\gamma_1 I-\phi I+\varepsilon\,(I(0)-I(t_f))\,exp(-\varepsilon t)) \\
&\leq \phi_1(t)\,(k(x,t)-k(x,t)sgn(\phi_1(t))-c_1 sgn(\phi_1(t))) \\
&\quad +\phi_2(t)\,(l(x,t)-l(x,t)sgn(\phi_2(t))-c_2 sgn(\phi_2(t))) \\
&= (k(x,t)\,|\phi_1(t)|-g_1(x,t)\,|\phi_1(t)|)-(l(x,t)\,|\phi_2(t)|-g_2(x,t)\,|\phi_2(t)|) \\
&= -c_1\,|\phi_1(t)|-c_2\,|\phi_2(t)| \leq 0.
\end{aligned}$$

By applying assumptions (i)-(iii), it is shown that $V(t) \neq 0$ remains strictly negative. Therefore, based on Lyapunov's stability theorem [31], the conditions $\phi_1(t)=\phi_2(t)=0$ exhibit asymptotic stability, which implies that both $\phi_1(t)$ and $\phi_2(t)$ gradually approach zero as t tends to infinity. Thus, the sliding mode control approach asymptotically leads to reducing the tracking error to zero.

Based on these results, $S(t) \to S_d(t)$ and $I(t) \to I_d(t)$ for $t \to \infty$, resulting in the eventual reduction of both susceptible and infected individuals to zero. As stated in Proposition 3.1, the objective of applying sliding mode control to minimize the overall number of COVID-19 cases is achieved even under parameter uncertainty. However, one limitation of this methods is that the upper bounds $k(x,t)$ and $l(x,t)$ on assumptions (i) and (ii) must be known beforehand for defining the switching gain (on the assumption (iii)) that depends on these values.

3.2. Adaptive gain adjustment in sliding mode control

This part describes an adaptive method to address the upper bounds on assumptions (i) and (ii). The switching control equation is changed to

$$\hat{u}_{1sw}(t) \quad = \quad \tfrac{1}{S(t)}\hat{g}_1(t)sgn\left(\phi_1(t)\right), \tag{20}$$

$$\hat{u}_{2sw}(t) \quad = \quad \tfrac{1}{I(t)}\hat{g}_2(t)sgn\left(\phi_2(t)\right), \tag{21}$$

so that the control laws equation (20) and (21) becomes

$$u_1(t) = \frac{1}{S(t)}\left(\Lambda - \left(\hat{q}S(t) + \varepsilon\left(S(0) - S(t_f)\right)\exp\left(-\varepsilon t\right)\right)\right) + \frac{\hat{g}_1(t)}{S(t)} sgn\left(\phi_1(t)\right), \tag{22}$$

$$u_2(t) = \frac{1}{I(t)}\left(\hat{r} - \left(\hat{s}I(t) + \varepsilon\left(I(0) - I(t_f)\right)\exp\left(-\varepsilon t\right)\right)\right) + \frac{\hat{g}_2(t)}{I(t)} sgn\left(\phi_2(t)\right). \tag{23}$$

Accordingly, the adaptive rules governing the update of the switching gain ($\hat{g}_1(t)$ and $\hat{g}_2(t)$) are formulated as follows:

$$\dot{\hat{g}}_1(t) = \Gamma\phi_1(t) sgn\left(\phi_1(t)\right)\Gamma\left|\phi_1(t)\right|, \quad \hat{g}_1(0) = 0, \tag{24}$$

$$\dot{\hat{g}}_2(t) = \Gamma\phi_2(t) sgn\left(\phi_2(t)\right)\Gamma\left|\phi_2(t)\right|, \quad \hat{g}_2(0) = 0, \tag{25}$$

where $\Gamma > 0$.

The switching gain $\hat{g}_1(t)$ and $\hat{g}_2(t)$ may be divergent considering that the derivatives of Equations (24) and (25) are non-negative definite. To ensure that the tracking error approaches zero, positive constants $\bar{k}$ and $\bar{l}$ from assumption (iv) are employed despite their unknown values. Thus, the two switching gain values increase until the upper bounds in Equations (16) and (17) are reached or $\hat{g}_1(t) \leq \bar{k}$ and $\hat{g}_2(t) \leq \bar{l}$. Subsequently, the system approaches a sliding surface, leading to the condition where $\phi_1(t) = \phi_2(t) = 0$, thus halting the further increase in the switching gain value. This approach ensures the attainment of the control objective, as outlined in Proposition 2.

Proposition 3.2. *If we consider the system (1) by applying the control (22) and (23), and assumptions (i) and (iv) apply to finite upper bounds $\bar{k}$ and $\bar{l}$ that are not yet known with certainty, and $\Gamma > 0$, then the tracking error will converge asymptotically to zero.*

To validate Proposition 3.2, assume that condition (iv) is satisfied. Consequently, there exist constants a such that $a \geq \bar{k} + c_1$ and b such that $b \geq \bar{l} + c_2$ for any given constants $c_1, c_2 > 0$. Based on this, the Lyapunov candidate function $L(t)$ is formulated as follows:

$$L(t) = \frac{1}{2}\left(\phi_1^2(t) + \phi_2^2(t) + \frac{1}{\Gamma}(\hat{g}_1(t) - a)^2 + \frac{1}{\Gamma}(\hat{g}_2(t) - b)^2\right). \tag{26}$$

Accordingly, the time derivative of Equation (26) is obtained as follows

$$\begin{aligned}\dot{L}(t) &= \phi_1(t)\dot{\phi}_1(t) + \phi_2(t)\dot{\phi}_2(t) + \frac{1}{\Gamma}(\hat{g}_1(t) - a)^2\dot{\hat{g}}_1(t) + \frac{1}{\Gamma}(\hat{g}_2(t) - b)^2\dot{\hat{g}}_2(t)\\ &\leq -c_1|\phi_1^2(t)| - c_2|\phi_2^2(t)| \leq 0.\end{aligned}$$

Furthermore, convergence towards the sliding surface is achieved by applying Barbalat's Theorem [31].

Consequently, Proposition 2 guarantees that implementing a sliding mode control strategy can efficiently decrease the populations $S(t)$ and $I(t)$ at a specific moment, even under parameter uncertainty. This effectiveness arises from the method's reliance on a reference function that gradually converges to zero over time.

4. SIMULATION

4.1. Numerical methods

This subsection introduces the algorithm used to conduct computational simulations for addressing the control challenge described in model (1). We compare the numerical results between scenarios without control and scenarios with control in model (1). Numerical solutions can be applied to address the adaptive sliding mode control problem in section 3, where S and I tend to zero by following their respective reference functions despite the presence of parameter uncertainty.

This control problem is solved by the following algorithm:

(i) Initialization of parameters and initial values: Utilize the values listed in Table 1 for the parameters along with the provided initial values.

(ii) Intervals for nominal parameters $\hat{\beta}$, $\hat{\beta_m}$, $\hat{\alpha_1}$, and $\hat{\gamma_1}$, where $\beta_L \leq \hat{\beta} \leq \beta_U$, $\beta_{mL} \leq \hat{\beta_m} \leq \beta_{mU}$, $\alpha_{1L} \leq \hat{\alpha_1} \leq \alpha_{1U}$, and $\gamma_{1L} \leq \hat{\gamma_1} \leq \gamma_{1U}$.

(iii) Divide the time interval $[0, t_f]$ into N subintervals of the same size to obtain intervals $[t_0 = 0, t_1], [t_1, t_2], \ldots, [t_{N-1}, t_N = t_f]$.
(iv) Set $i = 1$.
(v) Integrate the differential equation (1) by applying the fourth-order Runge-Kutta technique over the time steps $[t_{i-1}, t_i]$.
(vi) Define the reference functions $S_d(t_i)$ and $I_d(t_i)$ based on Equations (4) and (5). This function defines the targets of S and I to be achieved at each time point t.
(vii) Calculate tracking errors $e_1(t_i)$ dan $e_2(t_i)$.
(viii) Calculate the sliding mode control values $u_1(t)$ and $u_2(t)$ in Equations (22) and (23).
(ix) Determine the closed loop solution with the values u_1 and u_2 in step (v).
(x) Increase i by 1 and return to step (iv) repeatedly until reaching $i =$ N.
(xi) Sequence plots of S and I solutions without control and with control.

In step (ii), it is assumed that the parameters $\hat{\beta}$, $\hat{\beta_m}$, $\hat{\alpha_1}$, and $\hat{\gamma_1}$ are constrained by lower bounds: $\beta_L = \beta_{mL} = \alpha_{1L} = \gamma_{1L} = 0$, and upper bounds: $\beta_U = \beta_{mU} = \alpha_{1U} = \gamma_{1U} = 1$. If the lower limits are set a $\beta_L = \beta_{mL} = 0$, COVID-19 transmission does not occur. Conversely, when $\beta_U = \beta_{mU} = 1$, any susceptible person exposed will inevitably contract the infection. Setting $\alpha_{1L} = 0$, implies the absence of COVID-19 transmission, whereas an upper bound of $\alpha_{1U} = 1$, ensures that every interaction between a susceptible and an infected individual leads to infection. Additionally, if the parameter $\gamma_{1L} = 0$, infected individuals remain unrecovered, but when $\gamma_{1U} = 1$, they experience immediate recovery post-infection

The initial state values are set as follows: $S(0) = 8879574, E(0) = 1435275, E_m(0) = 67219$, $V(0) = 814656, I(0) = 15825, I_m(0) =, 4246, Q(0) = 1427, R(0) = 8386$. The total simulation duration spans 150 days, with parameter values estimated from Table 1, assigning $\Gamma = 0.1$. The following in Figure 3 is an application of Equations (4) and (5), with $\varepsilon = 0.5$.

4.2. Simulation of the adaptive sliding mode control

To demonstrate the impact of different optimal control approaches in managing the COVID-19 outbreak, three distinct strategies were applied, incorporating the control variables $u_1(t)$ and $u_2(t)$.

(a) Strategy 1: The provided input control is only vaccination ($u_1(t) \neq 0$ and $u_2(t) = 0$).
(b) Strategy 2: The provided input control is only isolation ($u_1(t) = 0$ and $u_2(t) \neq 0$).
(c) Strategy 3: The provided input control includes both vaccination and isolation ($u_1(t) \neq 0$ and $u_2(t) \neq 0$).

1) Strategy 1: The provided input control is only vaccination ($u_1(t) \neq 0$ and $u_2(t) = 0$): In strategy 1, Figure 3 (a) shows that after a vaccination control is applied, susceptible individuals begin to decline and follow the reference function after the 10th day. In Figure 3 (b) individuals who received vaccinations begin to increase after the control compared to before receiving the vaccination. Under Strategy 1, following the application of vaccine-based intervention, only a modest decline was observed in the number of individuals infected with both the original and Omicron variants when compared to the uncontrolled scenario. As depicted in Figure 3 (c), following the use of Strategy 1, the number of cases involving the original strain peaked at 611288 on day 11 prior to applying the intervention. However, following the implementation of vaccination control, this number declined to 581332. Meanwhile, the population infected with the Omicron variant reached a peak of infection on the 15th day of observation. Before the implementation of strategy 1 (Figure 3 (d)), the number reached 40402, while after the implementation of the control, this declined to 32487. Based on the control profile of strategy 1 shown in Figure 4 (a), we conclude that the vaccination control u_1 should be fully implemented (100%) from day 17 to day 68 and gradually reduced thereafter until reaching zero until the end of the simulation time.

2) Strategy 2: The provided input control is only isolation ($u_1(t) = 0$ and $u_2(t) \neq 0$): Under Strategy 2, the population infected with COVID-19 steadily declines to zero, in alignment with the reference function approaching zero. The implementation of isolation interventions successfully reduces COVID-19 cases by 88% As shown in Figure 3 (c), before the isolation policy was applied, the number of infections peaked

at 611293 on day 12 for those infected with the original strain. However, following the introduction of isolation, this figure dropped significantly to 19878. Similarly, cases involving the Omicron variant surged to 40403 on day 15 before declining sharply to 1599 as a result of isolation measures. According to the control profile illustrated in Figure 4 (b), isolation control u_2 should be maximally applied (100%) from the start until day 5, after which it should be progressively decreased to zero by the conclusion of the simulation on day 150.

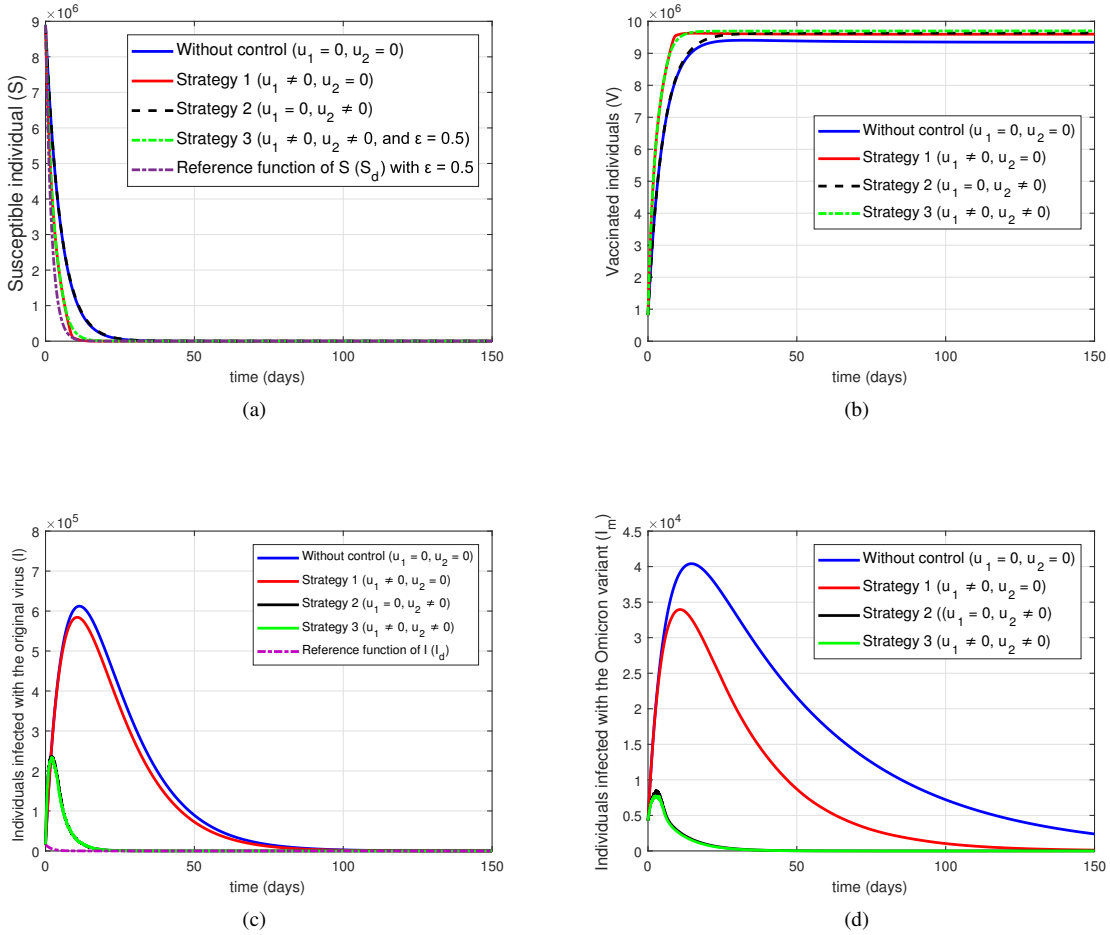

Figure 3: Population dynamics of S, V, I, and I_m.

3) Strategy 3: The provided input control includes both vaccination and isolation ($u_1(t) \neq 0$ and $u_2(t) \neq 0$): In strategy 3, as indicated by the simulation outcomes shown in Figure 3 (a), the combination of vaccination and isolation led to a reduction of 55.11% in the susceptible population. The population of susceptible individuals decreased asymptotically towards zero and reached the reference function (S_d) after the 15th day. As shown in Figure 3 (b) this led to a growth in the vaccinated grup (V). The individuals affected by the original strain of COVID-19 dropped to zero, aligning with the reference trajectory (I_d), which also tends toward zero (Figure 3 (c)). Based on the simulation, the original virus infections declined on average by 92.8%.According to Figure 3 (c), prior to implementing the control, infections peaked at 611891 on the 11th day; following the intervention, this number reduced substantially to 24828 (refer to Table 2). The decline in infections caused by the original virus was followed by a similar downward trend in Omicron case, as shown in Figure 3 (d). Before control strategies were applied, Omicron infections peaked

at 40296 on day 16. However, after implementing control measures, this figure dropped to 1296. The results from adaptive sliding mode control simulations showed an average decrease of 96.87% in the population infected with the Omicron strain. Referring to the control scheme illustrated in (Figure 4 (c)), vaccination efforts should begin on the first day and maintain maximum implementation (100%) from day 16 to day 68. In contrast, isolation measures are advised to be fully active (100%) from day 1 to day 4, then progressively reduced until fully withdrawn.

Table 2: A comparative analysis of people affected by the initial strain of the virus (I) and those classified as susceptible (S).

Days	**Individuals infected with the original virus (without control)**	**Individuals infected with the original virus (with control)**	**Susceptible individuals (without control)**	**Susceptible individuals (with control)**
1	147283	198457	7295099	5334707
2	255685	232793	5986094	3559580
3	344560	211991	4907175	2556045
4	416740	177335	4019351	1873549
⋮	⋮	⋮	⋮	⋮
10	607457	32707	1203121	10922
11	611891	24828	983404	3556
12	611289	19718	803673	1329
13	606436	15779	657136	656
14	598032	12232	537602	453
15	586696	9561	439683	391
⋮	⋮	⋮	⋮	⋮
90	5354	0	2226	365
91	4981	0	2226	365
92	4635	0	2226	365
93	4312	0	2226	365
⋮	⋮	⋮	⋮	⋮
149	74	0	2228	365
150	68	0	2228	364

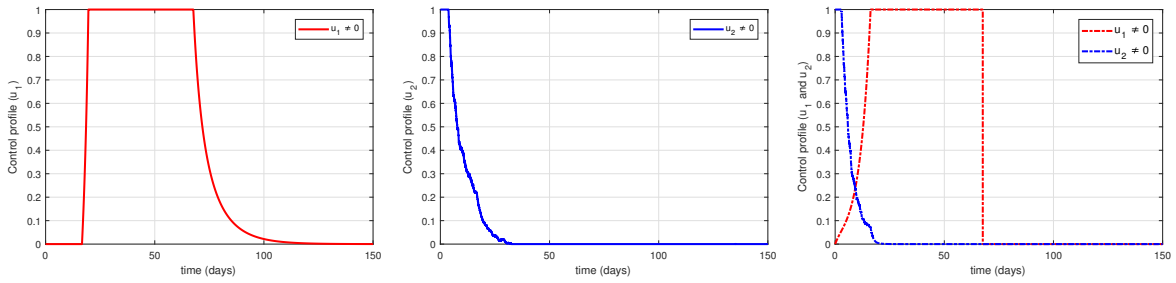

(a) (b) (c)

Figure 4: Visualization of the simulated control inputs for (a) strategy 1, (b) strategy 2, and (c) strategy 3.

4) Comparison of the three control strategies: Based on the strategy comparison analysis (see Table 3), strategy 3 yielded better results compared to strategies 1 and 2. Isolation control nearly reached the effectiveness of strategy 3 that combined vaccination and isolation. This suggests that a focus on controlling already infected individuals through isolation has a positive impact on disease prevention, while vaccination

Table 3: Evaluation of various control strategies.

Strategy	**Average Count of (S) (Susceptible) individuals**	**Average Count of (I) (Infected-Original)**	**Average Count of (I_m) (Infected-Omicron)**
Without control	299244	126169	16285
Strategy 1	163955	114731	8566
Strategy 2	302822	9503	546
Strategy 3	134342	9005	508

is more oriented towards preventing initial infection in susceptible populations. Without the controls, the number of susceptible individuals reached 299244, comprising 126169 individuals infected with the original virus and 16285 individuals infected with the Omicron variant. Strategy 1 (vaccination) resulted with both the original strain and the Omicron. In contrast, Strategy 2 (isolation) proved effective in lowering the cases of infection from both variants but did not significantly impact the number of S individuals. Overall, Strategy 3, which integrates both vaccination and isolation efforts, emerged as the most efficient approach to cubing the transmission of the original and Omicron variant.

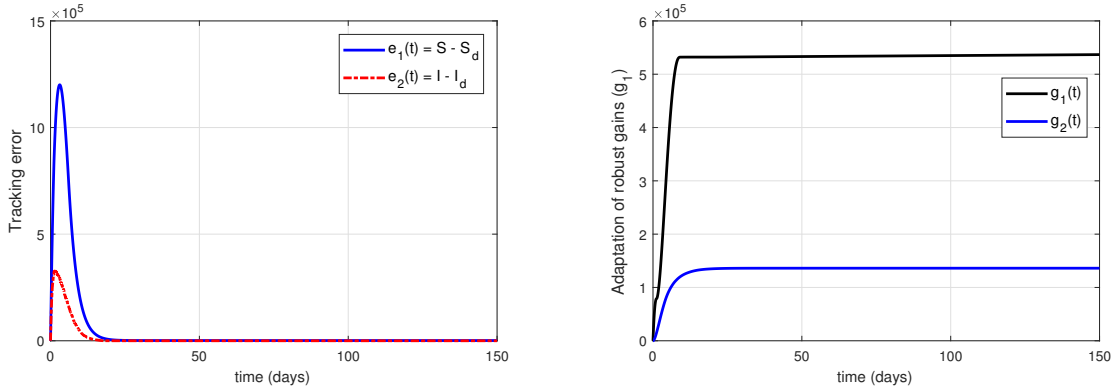

(a) (b)

Figure 5: Tracking errors of susceptible $(e_1 = S - S_d)$ and infected individuals $(e_2 = I - I_d)$, (b) The process of the gain $g_1(t)$ and $g_2(t)$ uses the adaptive law.

5) Effect of uncertainty on system performance: As shown in Figure 5 (a), the tracking errors $e_1(t)$ and $e_2(t)$ converge to zero, thereby achieving the control objective of diminishing the populations of $S(t)$ and $I(t)$ according to the given reference function. Figure 5 (b) shows the updated performance of the robustness of the gain $\hat{g}_1(t)$ and $\hat{g}_2(t)$ with adaptive control rules in Equations (24) and (25). The adaptive rule parameters (24) and (25) were chosen in such a way that the performance of the control is robust to model uncertainty. As shown in Figure 5 (b), gains $\hat{g}_1(t)$ and $\hat{g}_2(t)$ gradually increase until reaching an upper bound defined by (16) and (17) or $\hat{g}_1(t) \leq \bar{k}$ and $\hat{g}_2(t) \leq \bar{l}$. Subsequently, the system approaches a sliding surface, and $\phi_1(t) = \phi_2(t) = 0$ are reached so that the increase in the switching gain value stops (see subsection 3.2). This adjustment of the gain enhances the control's robustness against model uncertainty and guarantees the stability of the system.

In strategy 3, we then allow variation in the reference function convergence rate values for susceptible individuals (S), $\varepsilon = 0.3$ and $\varepsilon = 0.5$ as well as the convergence rate values for infected individuals (I), $\varepsilon = 0.03$ and $\varepsilon = 0.5$. The influence of selecting different values of the exponential convergence rate on the tracking error and the dynamics of susceptible and infected individuals can then be examined. Figure 6 (a)-(b) illustrates a faster decline in the populations S and I,driven by the swift convergence of the reference

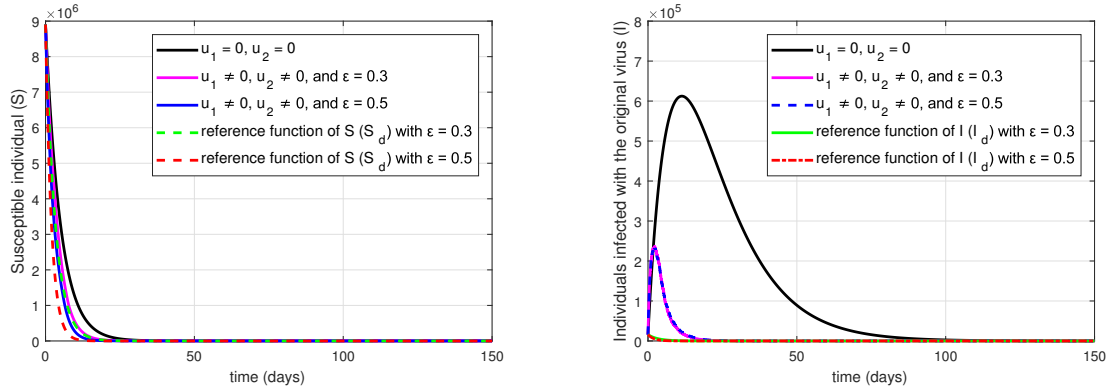

Figure 6: (a) Susceptible population trajectories $S(t)$ under various control inputs and reference function parameters, and (b) Original virus-infected population $I(t)$ dynamics with respect to ε variations in different strategies.

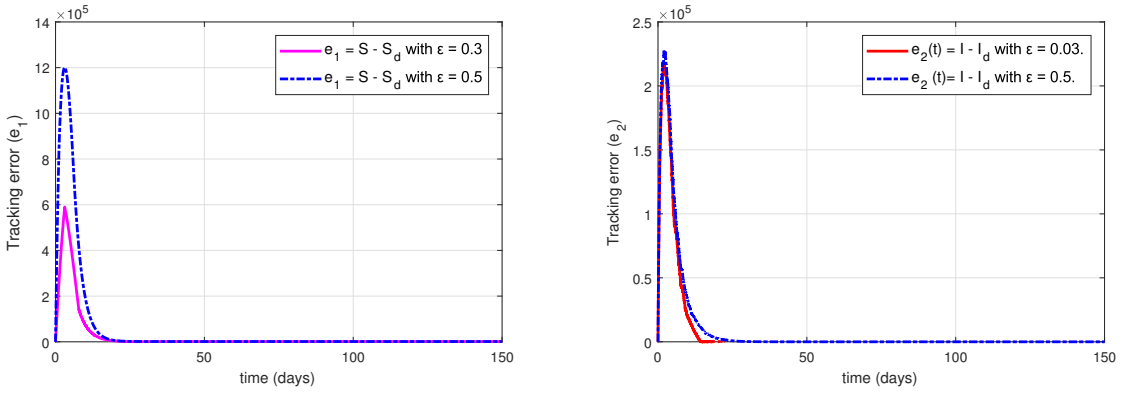

Figure 7: (a) Plot of the tracking error (e_1) corresponding to changes in ε for S_d, and (b) Plot of error (e_2) in response variations in ε for I_d.

trajectory. Nevertheless, it should be emphasized that a swift reduction in the number of infected individuals does not always imply a quicker minimization of the tracking error, as shown in Figure 7 (a)-(b). Simulation findings suggest that this control method is capable of addressing uncertainties in the Omicron-mutated COVID-19 model.

Within this study, the parameter uncertainty is confined within bounds, specifically set between a lower bound of 0 and an upper bound of 1, as detailed in Subsection 4.1. As a result, in Figure 8 (a)-(b)) the tracking error graphs $e_1(t)$ and $e_2(t)$ decrease to zero, although there is variation in parameter uncertainty. Support for this is also evident from the control profile (Figure 4), which indicates that chattering can be completely reduced, thus enhancing control effectiveness. This highlights the robustness and effectiveness of the adaptive sliding mode control method in meeting regulation goals, particularly in minimizing the numbers of susceptible and infected individuals by following a reference signal, even under uncertain parameter conditions.

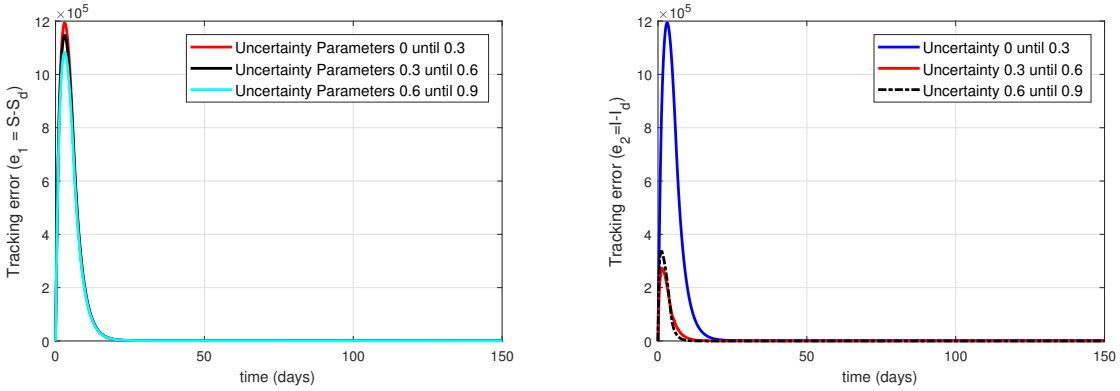

Figure 8: (a) Tracking error graph (e_1) with parameter uncertainty and (b) Tracking error graph (e_2) with parameter uncertainty.

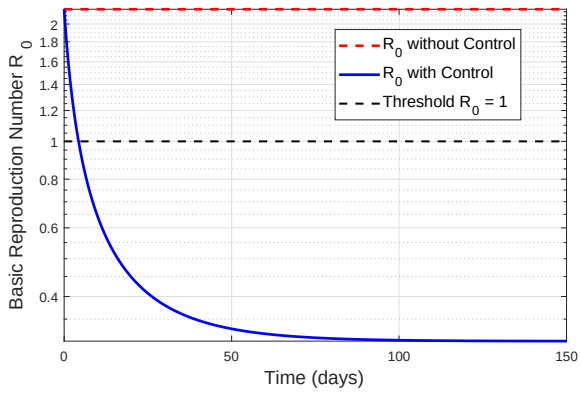

Figure 9: Reproduction number with and without control sliding mode adaptif.

Figure 9 illustrates the evolution of the basic reproduction number R_0 over time with and without the implementation of adaptive control. The red dashed line represents R_0 in the absence of control, maintaining a constant value above 2.0, indicating a high potential for disease transmission. In contrast, the blue line shows the evolution of R_0 when the adaptive control strategy is applied. It is observed that R_0 decreases significantly over time, crossing the epidemic threshold of $R_0 = 1$ at approximately $t = 5$ days, and continues to decline towards a value close to zero. This demonstrates the effectiveness of the control strategy in reducing disease transmission.

The numerical results further support this observation. Initially, R_0 for the primary infection group starts at $R_{01} = 1.1839$, and for the secondary infection group, $R_{02} = 2.1824$. After applying control, R_{01} is reduced to 0.1783, while R_{02} is reduced to 0.3073, representing a significant 85.92% reduction in R_0. This highlights the impact of adaptive control in mitigating disease spread by effectively lowering the reproduction number below the epidemic threshold. These results suggest that implementing an adaptive control strategy can effectively suppress the spread of infection within a short period. By adjusting control measures dynamically, the disease transmission can be contained efficiently, preventing large-scale outbreaks and supporting public health interventions.

6) Cost-Effectiveness Analysis: The Cost-Effectiveness Ratio (CER) quantifies the efficiency of an intervention by evaluating the resources required to prevent infections. It is mathematically expressed as

$$CER = \frac{C_{\text{total}}}{E_{\text{total}}}, \tag{27}$$

where C_{total} represents the total intervention cost, and E_{total} is the number of infections averted. A lower CER indicates a more cost-efficient strategy, as fewer resources are needed per prevented infection.

The total intervention cost C_{total} accounts for the expenses associated with vaccination and isolation measures

$$C_{\text{total}} = w_v \int_0^T u_1(t)\, dt + w_i \int_0^T u_2(t)\, dt, \tag{28}$$

where w_v and w_i denote the unit costs of vaccination and isolation respectively, and T represents the total simulation duration. The effectiveness of the intervention is computed as the difference between infections in the uncontrolled and controlled systems

$$E_{\text{total}} = \min\left(\int_0^T (I_{\text{uncontrolled}}(t) - I_{\text{controlled}}(t))dt, N \right), \tag{29}$$

where $I_{\text{uncontrolled}}$ and $I_{\text{controlled}}$ represent the number of infections in the absence and presence of interventions respectively, and N is the total population cap. Table 4 presents an overview of the overall expenses and the number of avoided infections for both the initial strain of COVID-19 (I) and the Omicron variant (I_m). The analysis considers three intervention scenarios: vaccination only, isolation only, and an integrated strategy combining both vaccination and isolation.

Table 4: Cost-Effectiveness Analysis of different intervention strategies.

Strategy	**Cost** I	**Cost** I_m	**Infections Averted** (I)	**Infections Averted** (I_m)	**CER** (I)	**CER** (I_m)
Strategy 1	2,753,634.44	1,457,978.11	3,661,119.88	9,525,380.75	0.7513	0.2749
Strategy 2	1,457,978.11	504,596.83	1,934,349.10	9,812,277.28	0.2377	0.4049
Strategy 3	4,211,612.55	3,602,684.60	5,595,468.98	10,523,278.35	0.2856	0.3419

Table 4 provides an overview of the cost-effectiveness ratio (CER) outcomes for various intervention approaches, such as vaccination, isolation, and their integration. The table summarizes both the overall expenses and the estimated reduction in infection cases involving the original (I) and the Omicron type (I_m). The results indicate that isolation is the most cost-effective strategy for controlling the original virus, with a CER of 0.2377, compared to vaccination, which has a higher CER of 0.7513. This suggests that during the early stages of the pandemic, isolation was more effective in reducing infections. However, for the Omicron variant, vaccination becomes more cost-effective ($CER = 0.2949$) due to widespread immunity, whereas isolation remains the lowest-cost strategy with a CER of 0.1134. The combination of vaccination and isolation provides the highest effectiveness in preventing infections, achieving 11.25 million averted cases for both virus types. While its CER values (0.3749 for I and 0.3419 for I_m) are higher than isolation alone, the combination strategy balances cost and effectiveness, making it an optimal approach when resources allow. These findings suggest that isolation was initially the most efficient intervention, but vaccination became more cost-effective over time, particularly for Omicron.

To evaluate how cost-effectiveness one intervention is compared to another, the Incremental Cost-Effectiveness Ratio (ICER) is determined using formula [32]:

$$ICER = \frac{C_i - C_j}{E_i - E_j}, \tag{30}$$

where C_i and C_j represent the total costs of two different strategies, and E_i and E_j denote their respective effectiveness. The ICER determines whether an additional investment in a more expensive intervention yields a proportionate increase in effectiveness.

Table 5 presents a comparison of various intervention strategies based on their cost-effectiveness. In strategy A (u_1, u_2) evaluates the cost-effectiveness of vaccination (u_1) versus isolation (u_2). The ICER for the original

Table 5: Incremental Cost-Effectiveness Ratio (ICER) analysis.

Strategy Comparison	**ICER** (I)	**ICER** (I_m)
Strategy A (u_1, u_2)	1.0434	-
Strategy B (u_3, u_1)	-0.0521	0.1429

virus (I) is 1.0434, indicating that vaccination incurs higher costs per infection prevented compared to isolation. However, ICER for Omicron variant (I_m) is undefined (-) due to the comparable effectiveness of both strategies in preventing Omicron infections. This suggests that both vaccination and isolation provide similar effectiveness in controlling Omicron, which is reasonable given that by the time Omicron spread, much of the population had already acquired immunity through natural infection or vaccination. Since Omicron is highly transmissible but generally milder than previous variants, the impact of isolation and vaccination on reducing its spread remains similar, leading to an ICER of zero. Meanwhile, Strategy B (u_3, u_1) examines the cost-effectiveness of a combined vaccination and isolation strategy (u_3) compared to vaccination alone (u_1). The ICER for I is -0.0521, suggesting that adding isolation slightly reduces the cost per infection averted, making the combination more cost-effective than vaccination alone. For Omicron, the ICER is 0.1429, indicating that while the combination strategy is more effective than vaccination alone, it comes with a slightly higher cost per infection prevented. These results highlight that isolation was initially the most cost-effective strategy, but the combination of vaccination and isolation became more beneficial for Omicron, despite the added cost.

5. CONCLUSION

This study introduced an adaptive sliding mode control framework for epidemic modeling, specifically targeting the spread of the Omicron variant of COVID-19. Using real data from the DKI Jakarta Health Office, model parameters were estimated via a genetic algorithm, and the effectiveness of the proposed control strategy was validated through numerical simulations. The main aim was to minimize the number of infections caused by both the initial strain of COVID-19 and its Omicron variant, all while considering parameter uncertainty. Unlike fixed-parameter control strategies, adaptive sliding mode control dynamically adjusts control gains to compensate for parameter variations, ensuring convergence to a desired reference function. Theoretical guarantees in Propositions 1 and 2 confirm that despite parameter uncertainty, the system remains stable and follows the reference trajectory.

Simulation results demonstrated the effectiveness of adaptive sliding mode control in minimizing infections while optimizing vaccination and isolation measures. The implementation of Strategy 3, which combines vaccination and isolation, led to a 55.11% decrease in the number of susceptible individuals. Furthermore, infections caused by the original COVID-19 strain were reduced by 92.8%, while those from the Omicron variant declined by 96.87%. The basic reproduction number (R_0) was reduced by 85.92%, further validating the effectiveness of the proposed approach in controlling epidemic outbreaks.

Beyond its epidemiological impact, adaptive sliding mode control was also evaluated in terms of economic feasibility through cost-effectiveness ratio (CER) and incremental cost-effectiveness ratio (ICER). The CER value determined by dividing the combined expenses of vaccination and isolation by the number of cases averted, thus reflecting the efficiency of the intervention. The ICER, on the other hand, compared strategy 3 with other alternatives by evaluating the extra cost per additional infection prevented when implementing control actions based on the adaptive sliding mode approach. The results indicate that, despite requiring potentially higher initial costs due to dynamic parameter adjustments, adaptive sliding mode control demonstrates long-term cost saving by significantly reducing infections, lowering hospitalization rates, and minimizing healthcare burdens. These findings suggest that adaptive sliding mode control is not only epidemiological effective but also economically viable, offering policymakers a robust strategy for optimizing pandemic intervention measures.

These findings underscore the advantages of an adaptive, uncertainty-resilient control strategy in epidemic management. The ability to dynamically adjust control gains in response to parameter variations enhances robustness, ensuring system stability while maintaining effective disease suppression. Unlike traditional control methods that rely on fixed parameters, adaptive sliding mode control provides real-time adaptability, making it a more suitable approach for epidemic control scenarios where transmission dynamics are inherently

uncertain.

While this study provides valuable insights, it is subject to certain modeling assumptions, including a closed population and uncertainty within predefined parameter ranges. Future research should explore direct comparisons between adaptive and non-adaptive control strategies to further quantify the benefits of real-time gain adaptation. Additionally, incorporating stochastic effects and external disturbances into the model could further enhance its robustness in epidemic management. Expanding the analysis with more comprehensive datasets across different regions would strengthen policy recommendations for pandemic control strategies.

ACKNOWLEDGEMENT

Part of this research was financially supported by the Sumatera Institute of Technology (ITERA) Scholarship 2020-2024.

REFERENCES

[1] Khan, M.A. and Atangana A., Mathematical modeling and analysis of COVID-19: A study of new variant Omicron, Physica A: Statistical Mechanics and its Applications, 599(2022), p. 127452, 2022.

[2] WHO, WHO Classification of Omicron (B.1.1.529): SARS-CoV-2 Variant of Concern, WHO. https://www.who.int/news/item/26-11-2021-classification-of-omicron-(b.1.1.529)-sars-cov-2-variant-of-concern, Accessed on February 15, 2023.

[3] Manjunath, R., Gaonkar, S.L., Saleh, E.A.M. and Husain, K., A comprehensive review on Covid-19 Omicron (B.1.1. 529) variant, Saudi Journal of Biological Sciences, 29(9), p. 103372, 2022.

[4] Liang, S., Jiang, T., Jiao, Z. and Zhou, Z., A model simulation on the SARS-CoV-2 Omicron variant containment in Beijing, China, Intelligent Medicine, 3(1), pp. 10-15, 2023.

[5] Khan, M.A. and Atangana, A., Modeling the dynamics of novel coronavirus (2019-nCov) with fractional derivative, Alexandria Engineering Journal, 59(4), pp. 2379-2389, 2020.

[6] Li, A., Wang, Y., Cong, P. and Zou, X., Re-examination of the impact of some non-pharmaceutical interventions and media coverage on the COVID-19 outbreak in Wuhan, Infectious Disease Modelling, 6, pp. 975-987, 2021.

[7] Liu, K. and Lou, Y., Optimizing COVID-19 vaccination programs during vaccine shortages, Infectious Disease Modelling, 7(1), pp. 286-298, 2022.

[8] Lambora, A., Gupta, K. and Chopra, K., Genetic algorithm-A literature review, 2019 International Conference on Machine Learning, Big Data, Cloud and Parallel Computing (COMITCon), pp. 380-384, 2019.

[9] Windarto, Indratno, S.W., Nuraini, N. and Soewono, E., A comparison of binary and continuous genetic algorithm in parameter estimation of a logistic growth model, AIP Conference Proceedings, 1587(1), pp. 139-142, 2014.

[10] Yarsky, P., Using a genetic algorithm to fit parameters of a COVID-19 SEIR model for US states, Mathematics and Computers in Simulation, 185, pp. 687-695, 2021.

[11] Qiu, Z., Sun, Y., He, X., Wei, J., Zhou, R., Bai, J. and Du, S., Application of genetic algorithm combined with improved SEIR model in predicting the epidemic trend of COVID-19, China, Scientific Reports, 12(1), p. 8910, 2022.

[12] Bera, M.K., Kumar, P. and Biswas, R.K., Robust control of HIV infection by antiretroviral therapy: a super-twisting sliding mode control approach, IET Systems Biology, 13(3), pp. 120-128, 2019.

[13] Tran, D.T., Ba, D.X. and Ahn, K.K., Adaptive backstepping sliding mode control for equilibrium position tracking of an electrohydraulic elastic manipulator, IEEE Transactions on Industrial Electronics, 67(5), pp. 3860-3869, 2019.

[14] Jiao, H. and Shen, Q., Dynamics analysis and vaccination-based sliding mode control of a more generalized SEIR epidemic model, IEEE Access, 8, pp. 174507-174515, 2020.

[15] Assegaf, F., Saragih, R. and Handayani, D., Adaptive sliding mode control for cholera epidemic model, IFAC-PapersOnLine, 53(2), pp. 16092-16099, 2020.

[16] Santos, D.M.L., Rodrigues, V.H.P. and Oliveira, T.R., Epidemiological control of COVID-19 through the theory of variable structure and sliding mode systems, Journal of Control, Automation and Electrical Systems, 33(1), pp. 63-77, 2022.

[17] Ibeas, A., Shafi, M., Ishfaq, M. and Ali, M., Vaccination controllers for SEIR epidemic models based on fractional order dynamics, Biomedical Signal Processing and Control, 38, pp. 136-142, 2017.

[18] Brauer, F., Castillo-Chavez, C. and Feng, Z., Mathematical models in epidemiology, New York: Springer, 2019.

[19] Edwards, K.M., Maternal antibodies and infant immune responses to vaccines, Vaccine, 33(47), pp. 6469-6472, 2015.

[20] Suhika, D., Saragih, R., Handayani, D. and Apri, M., Optimal control strategies based on extended Kalman filter in mathematical models of COVID-19, International Journal of Electrical and Computer Engineering, 14(6), pp. 6300-6312, 2024.

[21] Kim, Y.R., Choi, Y.J. and Min, Y., A model of COVID-19 pandemic with vaccines and mutant viruses, Plos One, 17(10), p. e0275851, 2022.

[22] Onishchenko, G.G., Sizikova, T.E., Lebedev, V.N. and Borisevich, S.V., The Omicron variant of the SARS-CoV-2 virus as the dominant agent of a new risk of disease amid the COVID-19 pandemic, Herald of the Russian Academy of Sciences, 92(4), pp. 381-391, 2022.

[23] Mwalili, S., Kimathi, M., Ojiambo, V., Gathungu, D. and Mbogo, R., SEIR model for COVID-19 dynamics incorporating the environment and social distancing, BMC Research Notes, 13(1), p. 352, 2020.

[24] Madubueze, C.E., Dachollom, S. and Onwubuya, I.O., Controlling the spread of COVID-19: optimal control analysis, Computational and Mathematical methods in Medicine, 2020(1), p. 6862516, 2020.

[25] Zelenkov, Y. and Reshettsov, I., Analysis of the COVID-19 pandemic using a compartmental model with time-varying parameters fitted by a genetic algorithm, Expert Systems with Applications, 224, p. 120034, 2023.

[26] DKI Jakarta, Provincial Health Office, DKI Jakarta Covid-19 Monitoring Data. https://corona.jakarta.go.id/id, Accessed on March 30, 2022.

[27] BPS, Life expectancy by province and sex (Year) 2018-2020. https://www.bps.go.id/indicator/40/501/1/angka-harapan-hidup-ahh-menurut-provinsi-dan-jenis-kelamin.html, Accessed on July 31, 2021.

[28] Suhika, D., Roberd, S. and Handayani, D., Application of nonlinear robust sliding mode control on mathematical model for spreading of Covid-19, In AIP Conference Proceedings, 3095(1), 2024.

[29] Tregoning, J.S., Flight, K.E., Higham, S.L., Wang, Z. and Pierce, B.F., Progress of the COVID-19 vaccine effort: viruses, vaccines and variants versus efficacy, effectiveness and escape, Nature Reviews Immunology, 21(10), pp. 626-636, 2021.

[30] Chi, W.Y., Li, Y.D., Huang, H.C., Chan, T.E.H., Chow, S.Y., Su, J.H., Ferrall, L., Hung, C.F. and Wu, T.C., COVID-19 vaccine update: vaccine effectiveness, SARS-CoV-2 variants, boosters, adverse effects, and immune correlates of protection, Journal of Biomedical Science, 29(1), pp. 1-27, 2022.

[31] Khalil, H., Nonlinear Systems, 3rd Edition, New Jersey: Prentice Hall, 2002.

[32] Asamoah, J.K.K., Okyere, E., Abidemi, A., Moore, S.E., Sun, G.Q., Jin, Z., Acheampong, E. and Gordon, J.F., Optimal control and comprehensive cost-effectiveness analysis for COVID-19, Results in Physics, 33, p. 105177, 2022.